Journal of Solid State Chemistry 184 (2011) 1148–1152

Contents lists available at ScienceDirect

Journal of Solid State Chemistry

journal homepage: www.elsevier.com/locate/jssc

First-principles study of the electronic and magnetic properties of oxygen-deficient rutile TiO_2(1 1 0) surface

Jibao Lu, Kesong Yang, Hao Jin, Ying Dai *, Baibiao Huang

School of Physics, State Key Laboratory of Crystal Materials, Shandong University, Jinan 250100, People's Republic of China

ARTICLE INFO

Article history:
Received 11 January 2011
Received in revised form
16 March 2011
Accepted 18 March 2011
Available online 23 March 2011

Keywords:
First principle calculations
TiO_2 surface
Oxygen vacancy
Ferromagnetism
Double exchange

ABSTRACT

Based on first-principles electronic structure calculations we find that the bridging oxygen vacancies on the (1 1 0) surface is more favorable and may be responsible for the unexpected ferromagnetism in undoped rutile TiO_2. Our results show that the ferromagnetism largely originates from the *d* orbitals of low-charge-state Ti ions converted from Ti^{4+} ions induced by the surface oxygen vacancies. The second-nearest neighbors of these ions (fivefold coordinated Ti) also contribute to the total magnetic moments. The spins induced by the local oxygen vacancies form a ferromagnetic arrangement.

1. Introduction

In recent years, so-called "d^0" magnetism has attracted lots of attentions [1–7] because it challenges our conventional understanding on the origin of magnetism, i.e., the magnetism is induced by partially filled *d* or *f* orbitals. So far, the "d^0" magnetism has been found in two classes of semiconductor materials. One is 2*p*-light-element doped oxides and nitrides such as C- and N-doped TiO_2 [6*c*], ZnO [6*d*,6*e*] and MgO [6*f*], and the other is undoped oxides and nitrides in which the magnetism is thought to be originated from cation vacancies [2,4,7–9]. In our previous report [8], we have studied the electronic and magnetic properties of oxygen- and titanium-deficient undoped bulk TiO_2, respectively, and it was found that the Ti vacancy could cause a high-spin defect state and stable ferromagnetic coupling as in the case of previous study on HfO_2 and TiO_2, but the oxygen vacancy reduces two Ti^{4+} ions into Ti^{3+} (d^1) with a spin moment of 1.0 μ_B, and the two Ti^{3+} ions form a stable antiferromagnetic state. The latter means that the oxygen vacancy has no contribution to the ferromagnetism of undoped TiO_2. However, experimental results also show that ferromagnetic property of undoped TiO_2 is sensitive to the oxygen pressure in the growth process of samples and the amount of oxygen vacancies [5,10–13], and thus it is inferred that surface oxygen vacancies play a crucial role on the magnetic property of undoped TiO_2, which may be different from those in bulk materials. For rutile TiO_2, it is known that the (1 1 0) surface is more stable than other surfaces, and oxygen vacancies are the most common point defects on the surface [14]. Theoretical investigations [15–17] have revealed that the isolated V_O on rutile TiO_2(1 1 0) surface could induce spin-polarized gap states with local magnetic moments, while the magnetic coupling between the local oxygen vacancies, i.e., coupling between two adjacent V_O, was seldom reported and necessary to be studied in detail. Accordingly, in the present work, the magnetic ordering of the oxygen vacancies and the mechanism of the magnetic coupling are investigated.

A key issue is that the standard DFT calculations generally fail to describe systems with localized (strongly correlated) *d* electrons. Several developments have been made to treat these strongly correlated systems, among which the LDA+*U* (or GGA+*U*) approach was proposed to be a feasible method. We have introduced the on-site effective *U* parameter adopted for Ti 3*d* electrons [18] via the Dudarev formulation [19] implemented in VASP. The only free parameter in this formulation is the difference between the effective Coulomb and the effective exchange interactions $U=\overline{U}-\overline{J}$. The choice of the appropriate *U* value for the calculations of TiO_2 has been the subject of previous theoretical studies [8,20,21]. For calculations of the bulk TiO_2, Finazzi et al. [20] compared various DFT methods and found that the GGA+*U* with $U\approx 3$ eV method describes the energy gap and impurity state of this material very well. For calculations of the TiO_2 surface, Calzado et al. [21] investigated the effect of on-site effective *U* parameter on the band-gap states of the reduced rutile (1 1 0) TiO_2 surface and proposed that the LDA+*U* method with the optimal *U* of 5.5 ± 0.5 eV could describe this reduced surface objectively. Moreover, in our previous work [8] we compared the LDA+*U* with the GGA+*U* calculations and found that this two methods yield similar results on the magnetic properties of the bulk oxygen-deficient TiO_2.

* Corresponding author.
E-mail addresses: daiy60@sina.com, daiy60@sdu.edu.cn (Y. Dai).

0022-4596/$ - see front matter © 2011 Elsevier Inc. All rights reserved.
doi:10.1016/j.jssc.2011.03.037

Nevertheless, in view of the fact that the system presently studied is the TiO_2 (1 1 0) surface (not the bulk), we employed the LDA+U method proposed in Ref. [21] to study the electronic and magnetic properties of this surface, and the GGA+U calculations was also carried out as a comparison [22].

2. Computational details

Our first-principles LDA+U ($U=\overline{U}-\overline{J}=5.8$ eV) [19–21] calculations were carried out by the Vienna *ab initio* simulation package [23] (note that the reliability of U=5.8 eV for LDA+U calculations on rutile (1 1 0) TiO_2 surface has been demonstrated explicitly by Calzado et al. Ref. [21].) and the GGA+U calculations was also carried out as a comparison [22]. The projector augmented plane-wave method [23], the plane-wave cutoff energy 500 eV and a Gamma centered $2\times2\times1$ k-point set were used [15,24]. The geometry relaxation cycles were terminated when all atomic force components were smaller than 0.01 eV/Å.

We modeled the TiO_2(1 1 0) surface by a 192-atom (4×2) [15] reconstruction surface cell consisting of four TiO_2 trilayers [15,25] (12 atomic layers, see Fig. 1(a)). The thickness of vacuum layer above the slab was 15 Å, and the vacuum spacing, corresponding to the width of about 5 trilayers, is found to be well converged. The atoms in the bottom trilayer were fixed at the optimized bulk positions and the other three trilayers were fully relaxed during the geometry optimizations.

3. Results and discussions

3.1. Relative stability

One bridging oxygen atom at the 1 position (see Fig. 1) is removed from the perfect TiO_2(1 1 0) surface to model the oxygen-deficient surface, which corresponds to a concentration of 12.5% of the bridging oxygen defect on the surface. It is sufficient to mimic the experimental value of the defect density (5–10%, see Refs. [26, 27]) and nicely corresponds to previous theoretical work [15]. Furthermore, this model has been shown to minimize the well-known energy oscillations as a function of the number of layers (even–odd) [25], and has been proved to consistent very well with the recent (LEED-IV) [28,29] experiment. To evaluate the relative stability of oxygen vacancy (V_O) and titanium vacancy (V_{Ti}) in the (1 1 0) surface of rutile TiO_2, we calculated their formation energies according to the following formula:

$$E_f = E_{def} - E_{pure} + \mu_x, \quad (1)$$

where E_{def} (E_{pure}) is the total energy of the rutile TiO_2 with (without) defects and μ_x is the chemical potential of O (μ_O) or Ti (μ_{Ti}) which reflects the elemental partial pressure of each element determined by the equilibrium growth conditions. Under extreme O-rich conditions, the oxygen chemical potential is assumed to be in equilibrium with O_2 molecule, and then the titanium chemical potential are obtained from the thermodynamic stability condition for their oxides

$$\mu_{Ti} + 2\mu_O = \mu_{TiO_2}, \quad (2)$$

where μ_{TiO_2} is the chemical potential of rutile TiO_2. Under extreme O-poor conditions, the titanium chemical potential is given by the energy of bulk metallic titanium, and likewise, the oxygen chemical potential is calculated from the stability condition of Eq. (2). Under moderate growth conditions, the oxygen and titanium chemical potential are constrained by Eq. (2).

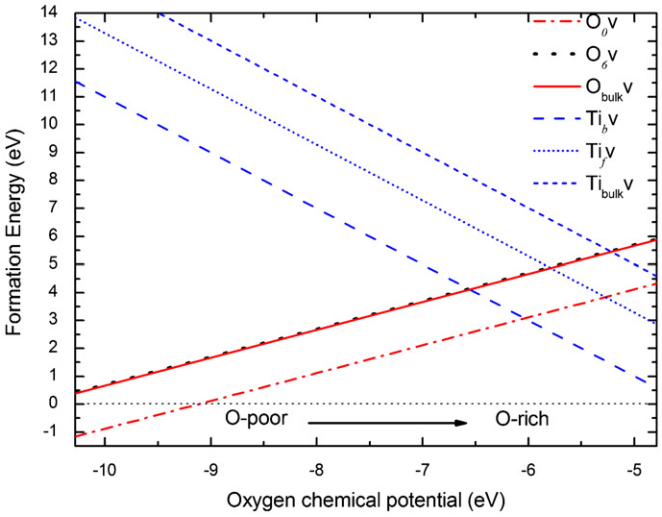

Fig. 2. Formation energies of an isolated oxygen(titanium) vacancy on the (1 1 0) surface. O_0v, O_6v, Ti_bv, and Ti_fv represent the vacancy generated by removing one of the atoms labeled in Fig. 1(b), respectively, and $O(Ti)_{bulk}$v represents the isolated vacancy in the bulk. The titanium chemical potential corresponding with the oxygen chemical potential can be obtained from Eq. (2).

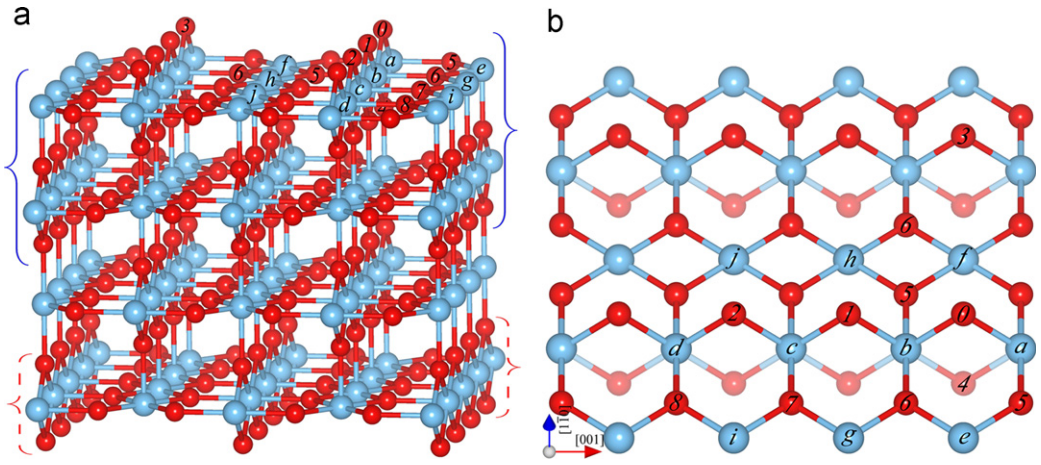

Fig. 1. (a) A Side view, (b) A 45° top view of the 192-atom 4×2 surface cell representing the slab of four TiO_2 trilayers (12 atomic layers) used to mimic the (1 1 0) surface of rutile TiO_2. In (b), only the top three atomic layers are shown. The labels are used to represent the relevant atoms. The larger sky blue and the smaller red spheres represent Ti and O atoms, respectively. (For interpretation of the references to color in this figure legend, the reader is referred to the web version of this article.)

The formation energies of various vacancies on surface and in bulk calculated as a function of the μ_O are shown in Fig. 2, from which we could obtain the following conclusions:

(1) The oxygen vacancy at the bridging site on the surface is energetically more favorable to form than in the bulk because of the lower formation energy, which is in agreement with the results of Ref. [30].
(2) The formation energy of titanium vacancy on the surface is also smaller than that in the bulk TiO_2, probably due to the decreased coordination of Ti_f and the outward moving of Ti_b on the surface.
(3) For surface V_O and V_{Ti}, the formation energy of oxygen vacancy on the surface at 0 and 6 sites (see Fig. 1(b)) is always lower than that of Ti vacancy at *b* and *f* sites on the surface under both O-rich and O-poor conditions, and similar trend is also found for V_O and V_{Ti} of bulk TiO_2. Therefore, the probability for V_O should be greater than that for V_{Ti} on the surface layer.

3.2. Electronic properties and magnetic coupling

The total densities of states (TDOS) of the pure and oxygen-deficient TiO_2(1 1 0) surface are shown in Fig. 3. The projected densities of states (PDOS) of the two top trilayers and the bottom trilayers of the perfect surface are also presented in Fig. 3(a). For the pure (1 1 0) TiO_2 surface, the calculated bandgap is about 1.8 eV, 0.7 eV smaller than that of the bulk rutile TiO_2 we calculated, mainly resulting from the surface states of the bottom trilayer, and interestingly, the energy gap of the first and second trilayers remains 2.5 eV, as shown in Fig. 3(a). The O 2*p* and Ti 3*d* states of the bottom trilayer are located at −0.5 to 0 eV and 1.8 to 2.0 eV, respectively, constituting the surface states. This probably originates from the fixed character of the bottom trilayer during relaxation (see Section 2), namely, since the bottom trilayer is fixed, the dangling bonds of the bridging O could not release their energy, leading to the up-shift of O 2*p* orbitals, and the increased charge transfer from the bridging O atoms to their nearby Ti atoms leads to the down-shift of the Ti 3*d* states. For the (1 1 0) surface with one isolated V_O, Fig. 3(b) shows that the spin-up defect states located at about 0.7 eV below the conduction band are introduced with the corresponding spin-down states lying in the conduction band, while the energy states of the perfect (1 1 0) surface are spin unpolarized (Fig. 3(a)). This is consistent with the previous experimental [31] and theoretical [15–17] reports. The partial density of states (PDOS) of 3*d* states of Ti ions around the V_O is plotted in Fig. 3(b) and the inset indicates that the band-gap states, largely composed of Ti 3*d* orbitals, are centered in $Ti^{(b),\ (c)}$, and $Ti^{(g),\ (h)}$. (Hereafter, Ti $^{(a)}$ stands for the Ti atom labeled "*a*" and $O^{(0)}$ stands for the O atom labeled "0" and so on.) Moreover, these magnetic moments induced by the isolated V_O form a paramagnetic arrangement (with very low exchange energy ($|\varepsilon| < 5$ meV)).

To study the coupling between the oxygen vacancies, two bridging oxygen atoms at the 0 and *i* (i=1–3) positions (see Fig. 1) are removed, leading to three possible different arrangements. For simplicity, the three arrangements are referred to as (0, *i*) (i=1–3) configurations. For each (0, *i*) configuration, the calculated energy difference between the antiferromagnetic (AFM) (see Fig. 4) and the ferromagnetic (FM) states, $\Delta E_M = E_{AFM} - E_{FM}$, with and without geometry relaxation, the relative stabilities, $\Delta E = E_{FM}(0, i) - E_{FM}(0, 1)$, of these configurations, and distances of the two O vacancies are listed in Table 1. The results reveal that the (0, 1) configuration is the most stable one among the three configurations.

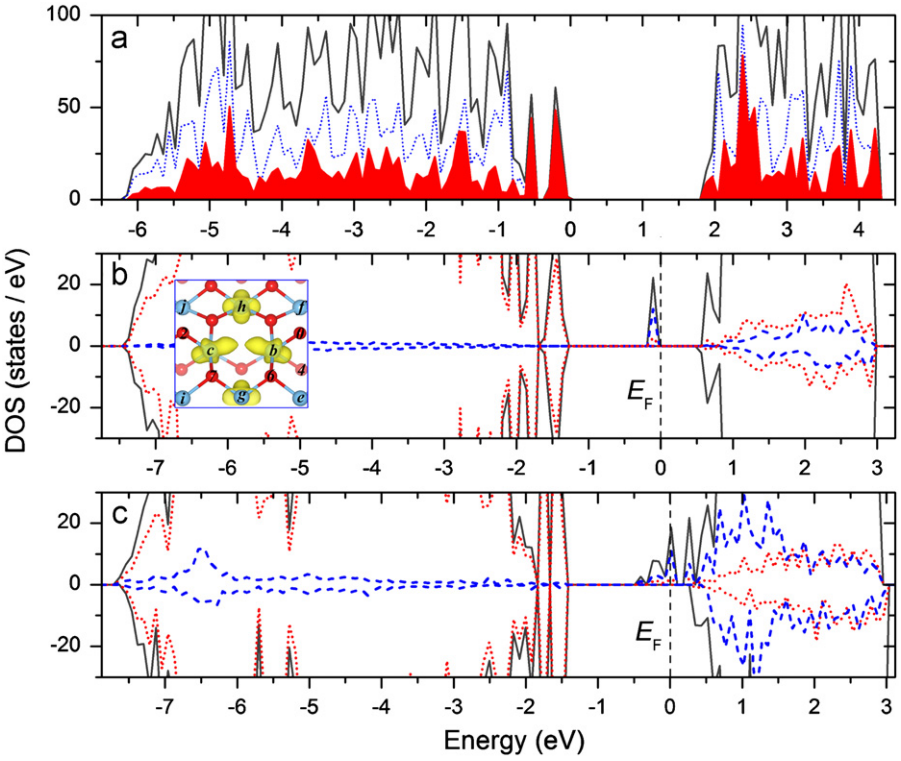

Fig. 3. (a) TDOS (solid line), PDOS (short dotted line) of the top two trilayers (the trilayers bounded in the solid braces in Fig. 1(a)) and PDOS (filled area) of the bottom trilayer (the trilayer bounded in the dashed braces in Fig. 1(a)) of the perfect rutile TiO_2(1 1 0) surface. Since the system is spin unpolarized, only the spin-up states are plotted. (b), (c) TDOS (solid line), PDOS (short dashed line) of 3*d* states of Ti around V_O and PDOS (short dotted line) of O 2*p* states of the isolated-V_O-deficient rutile TiO_2(1 1 0) surface (b), (0, 1) configuration (c). The inset of (b) indicates the spin densities localized on $Ti^{(b),\ (c),\ (g),\ (h)}$ (a 45° top view). The vertical dashed line denotes the Fermi level.

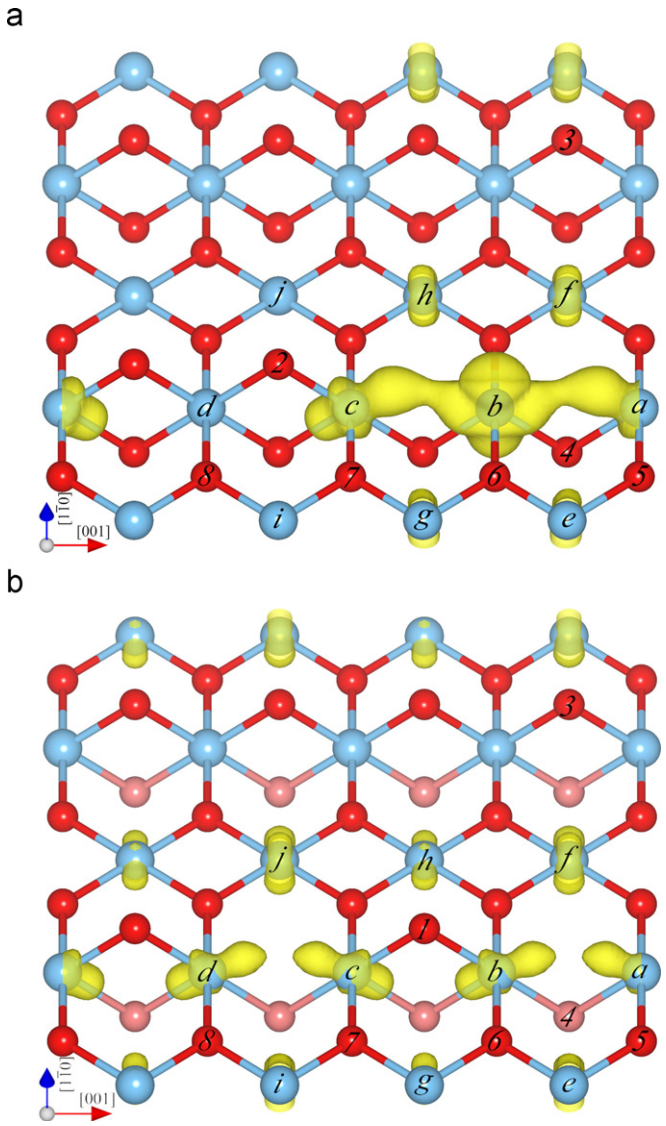

Fig. 4. Calculated spin densities on the Ti and O atoms for (0, 1) (a), (0, 2) (b), configurations (only the top three atomic layers are shown). The AFM geometry used in the calculation of the AFM magnetic energy is set as follows: 1. for (0, 1) configuration, two AFM geometries are considered: AFM_1: (bcgh)↑ (aef)↓; AFM_2: (acefgh)↑ b↓. 2. for (0, 2) configuration, one AFM geometry are considered: (cdij)↑ (abef)↓. The symbols of "↑" and "↓" represent the "spin-up" and "spin-down" sites, respectively. For (0, 1) configuration, the energy of AFM_1 was found to be smaller than that of AFM_2 and was used in the calculation in Table 1.

Table 1
Values of the relative stability, $\Delta E = E_{FM}(0, i) - E_{FM}(0, 1)$, the magnetic energy difference, $\Delta E_M = E_{AFM} - E_{FM}$, and the distance V_O–V_O between the O-vacancy sites (in the unrelaxed surface structure) of two O-vacancies on the (1 1 0) surface of rutile TiO_2 at LDA+U levels.

(0, i)	ΔE (meV)	ΔE_M (meV)	Coupling	V_O–V_O (Å)
(0, 1)	0	145 (2 0 4)[a] [83 (1 2 3)][b]	FM	2.963
(0, 2)	289	120 (1 2 4)	FM	5.926
(0, 3)	255	0.05(88)	(FM)	6.619

[a] The numbers in the parentheses are the values calculated from the unrelaxed surface structures derived from the bulk structure.
[b] The numbers in the square brackets are the values calculated by using standard DFT method.

Interestingly, for (0, 1) and (0, 2) configurations, the FM states are always more stable than the AFM states independent of the geometry relaxation, while the (0, 3) configuration becomes paramagnetic after the relaxation because of the too large distance between the two V_O. By taking all the three configurations into account, the oxygen-deficient TiO_2(1 1 0) surface should show a ferromagnetic property. To check the persistence of magnetic coupling in the system, we repeated the calculations using standard DFT method, and the calculated results clearly indicate that the ferromagnetic coupling between two V_O is energetically more favorable than the antiferromagnetic coupling, which indicates the coupling properties in this system is independent of the calculation methods (LDA+U or LDA). Therefore, we can conclude that the ferromagnetic coupling between the two V_O is intrinsic, which is in good agreement with the experimentally observed ferromagnetic-like behavior in oxygen-deficient TiO_2 systems [5,15–17,23].

The origin of ferromagnetism in Diluted Magnetic Semiconductors (DMS) has been widely discussed over the past years [32–37], and strongly depends on whether the system is metallic or insulating. If the system is metallic, the itinerant ferromagnetism is expected for the small concentration of carrier in the conduction band [38,39], which has similar origin to the double exchange interactions. However, if the system is insulating, the magnetic interactions are driven by the superexchange mechanism, and can be either ferro- or antiferromagnetic, depending on the orbital configuration. To explain the ferromagnetism of the TiO_2(1 1 0) surface with two local V_O, we show the TDOS and PDOS of (0, 1) configuration in Fig. 3(c). Different from the DOS of isolated V_O (Fig. 3(b)), the impurity band is broadened and the Fermi level is within the impurity band, resulting in a local half-metallic character. For the (0, 2) configuration, similar results are obtained. On the other hand, the double exchange mechanism requires the presence of magnetic ions with different electron occupancies. Simply speaking, the isolated V_O creates two Ti^{3+} ($d1$) ions, so there cannot be a double exchange mechanism. Interestingly, conditions are different for (0, 1) configuration. The two adjacent V_O's introduce two dangling bonds on $Ti^{(b)}$ and one dangling bond on $Ti^{(a)}$ and $Ti^{(c)}$, respectively (Fig. 4(a)). In principle, this makes $Ti^{(b)}$ a Ti^{2+} ion and $Ti^{(a),\,(c)}$ Ti^{3+} ions, and the double exchange coupling could occur between these ions with different electron occupancies. Moreover, the different maps of spin densities of the ions ($Ti^{(a),\,(c)}$ and $Ti^{(b)}$ in (0, 1) configuration, $Ti^{(f),\,(e)}$ and $Ti^{(g),\,(h)}$ in (0, 2) configuration) also indicate that their electron occupancies are different (Fig. 4). On the basis of the present analysis, the double exchange should be the dominant coupling mechanism for the ferromagnetism in this system.

4. Conclusion

In summary, our investigations indicate that the bridging oxygen vacancy of (1 1 0) surface, which forms easily under low oxygen partial pressure growth condition, introduces spin polarized localized states located at 0.7 eV below the conduction band edge and generates a magnetic moment of 2.0 μ_B. The double exchange interaction gives rise to a ferromagnetic coupling between the spins induced by the local V_O.

Acknowledgments

This work is supported by the National Natural Science foundation of China under Grants 10774091 and 20973102, National Basic Research Program of China (973 Program, Grant 2007C B613302), and the Natural Science Foundation of Shandong Province under Grant Y2007A18. H. Jin would like to thank Dr. Wei Fan and Dr. Hu Xu (Technical Institute of Physics and Chemistry, China) for useful discussions.

Appendix A. Supplementary materials

Supplementary data associated with this article can be found in the online version at doi:10.1016/j.jssc.2011.03.037.

References

[1] R. Monnier, B. Delley, Phys. Rev. Lett. 87 (2001) 157204.
[2] S. ElfimovI, S. Yunoki, G.A. Sawatzky, Phys. Rev. Lett. 89 (2002) 216403.
[3] M. Venkatesan, C.B. Fitzgerald, J.M.D. Coey, Nature (London) 430 (2004) 630.
[4] C. Das Pemmaraju, S. Sanvito, Phys. Rev. Lett. 94 (2005) 217205.
[5] N.H. Hong, J. Sakai, N. Poirot, V. Brizé, Phys. Rev. B 73 (2006) 132404.
[6] (a) M.A. Garcia, et al., Nano Lett. 7 (2007) 1489;
(b) H. Peng, H.J. Xiang, S.H. Wei, S.S. Li, J.B. Xia, J. Li, Phys. Rev. Lett. 102 (2009) 017201;
(c) J.G. Tao, L.X. Guan, J.S. Pan, C.H.A. Huan, L. Wang, J.L. Kuo, Z. Zhang, J.W. Chai, S.J. Wang, Appl. Phys. Lett. 95 (2009) 062505;
(d) H. Pan, J.B. Yi, L. Shen, R.Q. Wu, J.H. Yang, J.Y. Lin, Y.P. Feng, J. Ding, L.H. Van, J.H. Yin, Phys. Rev. Lett. 99 (2007) 127201;
(e) K.S. Yang, R.Q. Wu, L. Shen, Y.P. Feng, Y. Dai, B.B. Huang, Phys. Rev. B 81 (2010) 125211;
(f) B. Gu, N. Bulut, T. Ziman, S. Maekawa, Phys. Rev. B 79 (2009) 024407;
(g) Z.K. Zhang, Y. Dai, B.B. Huang, M.H. Whangbo, Appl. Phys. Lett. 96 (2010) 062505.
[7] H. Jin, Y. Dai, B.B. Huang, M.H. Whangbo, Appl. Phys. Lett. 94 (2009) 162505 Virtual J. Nanoscale Sci. & Tech., May 4 (2009).
[8] K.S. Yang, Y. Dai, B.B. Huang, Y.P. Feng, Phys. Rev. B 81 (2010) 033202.
[9] H. Peng, J. Li, S.S. Li, J.B. Xia, Phys. Rev. B 79 (2009) 092411.
[10] A.K. Rumaiz, B. Ali, A. Ceylan, M. Boggs, T. Beebe, S.I. Shah, Solid State Commun. 144 (2007) 334.
[11] A. Hassini, J. Sakai, J.S. Lopez, N.H. Hong, Phys. Lett. A 372 (2008) 3299.
[12] C. Sudakar, P. Kharel, R. Suryanarayanan, J.S. Thakur, V.M. Naik, R. Naik, G. Lawes, J. Magn. Magn. Mater. 320 (2008) L31.
[13] S. Zhou, E. Čižmár, K. Potzger, M. Krause, G. Talut, M. Helm, J. Fassbender, S.A. Zvyagin, J. Wosnitza, H. Schmidt, Phys. Rev. B 79 (2009) 113201.
[14] U. Diebold, Surf. Sci. Rep. 48 (2003) 53.
[15] C. DiValentin, G. Pacchioni, A. Selloni, Phys. Rev. Lett. 97 (2006) 166803.
[16] T. Bredow, G. Pacchioni, Chem. Phys. Lett. 355 (2002) 417.
[17] W.C. Mackrodt, E.A. Simson, N.M. Harrison, Surf. Sci. 384 (1997) 192.
[18] V.I. Anisimov, J. Zaanen, O.K. Andersen, Phys. Rev. B 44 (1991) 943.
[19] S.L. Dudarev, G.A. Botton, S.Y. Savrasov, C.J. Humphreys, A.P. Sutton, Phys. Rev. B 57 (1998) 1505.
[20] E. Finazzi, C.D. Valentin, G. Pacchioni, A. Selloni, J. Chem. Phys. 129 (2008) 154113.
[21] C.J. Calzado, N.C. Hernández, J.F. Sanz, Phys. Rev. B 77 (2008) 045118.
[22] See supporting information at doi:10.1016/j.jssc.2011.03.037 for the results of the GGA+U calculations.
[23] G. Kresse, D. Joubert, Phys. Rev. B 59 (1999) 1758.
[24] H.J. Monkhorst, J.D. Pack, Phys. Rev. B 13 (1976) 5188.
[25] T. Bredow, L. Giordano, F. Cinquini, G. Pacchioni, Phys. Rev. B 70 (2004) 035419.
[26] U. Diebold, J. Lehman, T. Mahmoud, M. Kuhn, G. Leonardelli, W. Hebenstreit, M. Schmid, P. Varga, Surf. Sci. 411 (1998) 137.
[27] M.A. Henderson, Surf. Sci. 355 (1996) 151.
[28] R. Lindsay, A. Wander, A. Ernst, B. Montanari, G. Thornton, N.M. Harrison, Phys. Rev. Lett. 94 (2005) 246102.
[29] S.J. Thompson, S.P. Lewis, Phys. Rev. B 73 (2006) 073403.
[30] H. Cheng, A. Selloni, J. Chem. Phys. 131 (2009) 054703.
[31] V.E. Henrich, G. Dresselhaus, H.J. Zeiger, Phys. Rev. Lett. 36 (1976) 1335.
[32] H. Ohno, Science 281 (1998) 951.
[33] I. Žutić, J. Fabian, S.D. Sarma, Rev. Mod. Phys. 76 (2004) 323.
[34] A.J. Behan, A. Mokhtari, H.J. Blythe, D. Score, X.H. Xu, J.R. Neal, A.M. Fox, G.A. Gehring, Phys. Rev. Lett. 100 (2008) 047206.
[35] T. Dietl, H. Ohno, F. Matsukura, J. Cibert, D. Ferrand, Science 287 (2000) 1019.
[36] J.M.D. Coey, M. Venkatesan, C.B. Fitzgerald, Nat. Mater. 4 (2005) 173.
[37] H. Pan, Y.P. Feng, Q.Y. Wu, Z.G. Huang, J. Lin, Phys. Rev. B 77 (2008) 125211.
[38] V. Heine, J.H. Samson, J. Phys. F: Metal Phys. 10 (1980) 2609.
[39] V. Heine, J.H. Samson, J. Phys. F: Metal Phys. 13 (1983) 2155.